NASA TECHNICAL NOTE

NASA TN D-7957

NASA TN D-7957

CALCULATION OF CURRENT COLLECTED IN A DILUTE PLASMA THROUGH A PINHOLE IN THE INSULATION COVERING A HIGH-VOLTAGE SURFACE

Gustave C. Fralick

Lewis Research Center
Cleveland, Ohio 44135

NATIONAL AERONAUTICS AND SPACE ADMINISTRATION • WASHINGTON, D. C. • JUNE 1975

1. Report No. NASA TN D-7957	2. Government Accession No.	3. Recipient's Catalog No.
4. Title and Subtitle CALCULATION OF CURRENT COLLECTED IN A DILUTE PLASMA THROUGH A PINHOLE IN THE INSULATION COVERING A HIGH-VOLTAGE SURFACE		5. Report Date June 1975 6. Performing Organization Code
7. Author(s) Gustave C. Fralick		8. Performing Organization Report No. E-8186
9. Performing Organization Name and Address Lewis Research Center National Aeronautics and Space Administration Cleveland, Ohio 44135		10. Work Unit No. 505-04 11. Contract or Grant No.
12. Sponsoring Agency Name and Address National Aeronautics and Space Administration Washington, D.C. 20546		13. Type of Report and Period Covered Technical Note 14. Sponsoring Agency Code

15. Supplementary Notes

16. Abstract

A procedure is described for calculating the current collected by a pinhole defect in the insulation covering a high voltage surface. The results apply to a satellite at geosynchronous altitude where the effects of satellite motion and collective plasma effects on the collected current may be ignored.

17. Key Words (Suggested by Author(s))

Plasma interactions; Communications satellites; Space plasma; High voltage; Leakage; Pinholes; Space charge

18. Distribution Statement

Unclassified - unlimited
STAR Category 75 (rev.)

19. Security Classif. (of this report)	20. Security Classif. (of this page)	21. No. of Pages	22. Price*
Unclassified	Unclassified	35	$3.75

* For sale by the National Technical Information Service, Springfield, Virginia 22151

CALCULATION OF CURRENT COLLECTED IN A DILUTE PLASMA THROUGH A PINHOLE IN THE INSULATION COVERING A HIGH-VOLTAGE SURFACE

by Gustave C. Fralick

Lewis Research Center

SUMMARY

A procedure is described for calculating the current collected through a pinhole defect in the insulation covering a high-voltage surface. The results apply to a satellite at geosynchronous altitude where collective plasma effects and the motion of the satellite can be neglected in computing the currents.

The results indicate that the presence of the insulation around a pinhole reduces the current and that the experimentally observed current enhancement is probably due to surface leakage in the insulation.

INTRODUCTION

The use of high-voltage solar arrays on spacecraft to power devices such as radio-frequency amplifiers and ion thrusters promises more efficient spacecraft and less complicated electronics. The feasibility of using such arrays has been investigated (refs. 1 and 2). It was found that the possibility of large power losses due to current leakage to the space plasma, especially at lower altitudes, can be minimized by insulating the high-voltage surfaces. However, voids in the insulation and puncture by micrometeorites will result in high-voltage pinholes being exposed to the space plasma. There is evidence that these pinholes can collect unexpectedly large currents. Cole, Ogawa, and Sellan (ref. 3) found that the current collected is larger than can be accounted for by simple analytical models, as have Grier and McKinzie (ref. 4). These currents can result in a loss of power and in the formation of a high-temperature region at the site of the pinhole, which will lead to further deterioration of the insulation. Another effect, not fully understood, is the area effect reported by various observers (refs. 5 and 6). The effect of the insulation in these experiments is to actually enhance the current collection. The collected current appears to be more a function of the area

of the insulating surface surrounding the pinhole rather than a function of the pinhole area itself. This phenomena has been observed for various types of insulation.

Most of the analytical work in this area has been done by Parker and Whipple in their study of electrostatic probes on satellites (refs. 7 to 9). In their method currents are calculated by determining the trajectories of collected particles. They used two models for their calculations of probe currents. Their first model was a small circular equipotential surface, which represented the probe, surrounded by an infinite flat surface at zero potential, which represented the remainder of the satellite. In their second model the satellite was represented by a right circular cylinder with the probe being a small circular area in the center of one end of the cylinder. Published results using this model consider only the case where each surface is an equipotential.

In this report the effects of the insulation are incorporated by modeling the insulator with a nonequipotential surface surrounding the pinhole, which should be more realistic than using an equipotential surface. In addition, higher pinhole voltages are used, up to 10 kilovolts, rather than the lower voltages previously considered. These voltages are more representative of actual values. The calculations of the currents were performed using the trajectory tracing technique of Parker and Whipple. The goal of this study is to determine the effects of a nonequipotential surface surrounding the pinhole in the hope of providing an explanation of the area effect based solely on electrostatic effects.

MODEL

Geometrical Model

The geometrical model used to simulate a pinhole defect in the insulation covering a high voltage surface was simply two concentric disks (fig. 1). The inner disk represents the pinhole and is at a uniform potential. The annular region between the radii of the inner and outer disk represents the insulation. A typical voltage profile is shown in figure 2, which is based on measurements by Boeing (ref. 6). In all the calculations the diameter of the outer disk was 10.2 centimeters (4 in.). Two diameters were used for the pinhole, 0.38 centimeter (0.15 in.) and 0.57 centimeter (0.225 in.). This model is similar to the pinhole-insulation configurations used in testing in plasma tanks and to the test surfaces that were to have been used on the SPHINX (Space Plasma High voltage INteraction eXperiment) satellite (ref. 10).

Analytical Model

To calculate the pinhole current, it is necessary to know the voltage on the insula-

tion, as this is part of the boundary condition of the problem. But this voltage must be calculated. If an insulator is inserted into a plasma, the voltage at each point will change until an equal number of positive and negative charges per unit time are attracted from the plasma at each and every point on the insulator. If the voltage at a point is too positive, an excess number of electrons will be attracted, and the voltage will decrease until the electron and ion current densities are equal. In the same way, if the voltage is too negative, more ions will be attracted and the voltage will rise.

Ideally, then, the current densities should be calculated at each point on the insulator, and the voltage distribution adjusted until the current densities are equal. The voltage on the pinhole would remain constant at its specified value. However, a voltage change at one point on the disk would change the voltage distribution everywhere around the disk and the current everywhere else, not just at that point. This would lead to some sort of iterative technique for computing the insulator potential distribution, which may converge only slowly and could be very costly in terms of computer time.

Instead, it was felt that the magnitude of the effect of insulator voltage could be studied without having the "correct" voltage at each point on the insulator. The approach was to work with the plots of the equipotential lines surrounding the disk for various voltage distributions on the insulator and then to calculate the currents for the cases of interest. The plots could be generated relatively quickly.

The electric field was calculated assuming an infinite Debye length (Laplace field), and, although a magnetic field is included in the equations herein, all the currents were computed with $\vec{B} = 0$. In calculating particle trajectories, it was assumed that collisions with other particles could be ignored and that the plasma was nonstreaming. Thus, the results should be applicable to geosynchronous altitude, where high-voltage solar arrays could be used to power communications satellites. At this altitude, the Debye length is about 200 centimeters, the mean free path is of the order of several kilometers, and the thermal velocities of the ions and electrons are at least an order of magnitude greater than the speed of the satellite.

BRIEF DESCRIPTION OF SOLUTION

This section contains a short description of how the currents were calculated by tracing out particle trajectories and how the electrostatic field was calculated. A full description of the method of solution is given in appendix A. (Symbols are defined in appendix B.)

The normal component of the current density for a given species of particle at a point P on the disk is given by

$$j(\vec{r}_p) = q \iiint_{\text{allowed}} \vec{V} \cdot \hat{n} f(\vec{r}_p, \vec{V}) V^2 \, dV \sin \theta_V \, d\theta_V \, d\varphi_V$$

where q is the charge on the particle, $\vec{V}$ is the particle velocity, $\hat{n}$ is the unit normal at the current collection point, f is the distribution function in the six-dimensional phase space formed by the three particle coordinates and three components of velocity, $\vec{r}_p$ is the position vector of the current collection point, and θ_V and φ_V give the direction of $\vec{V}$ at P (see appendix A).

The method of solution makes use of the fact that, although the functional form of f is unknown at P, as long as collisions with other particles can be ignored and energy is conserved along particle trajectories, the numerical value of f is constant on a trajectory (refs. 6 to 8). At infinity, where the presence of the disk has essentially no effect on the space plasma, the distribution function is assumed to be a known function of the coordinates and velocity. Here, the distribution function is taken to be Maxwell-Boltzmann, which, for the case of a nonstreaming plasma considered in this analysis, has the form

$$f(\vec{r}_\infty, \vec{V}_\infty) = n_0 \left(\frac{m}{2\pi kT}\right)^{3/2} e^{-mV_\infty^2/2kT} = f(\vec{r}_p, \vec{V})$$

where $\vec{V}_\infty$ is the particle velocity at infinity, n_0 is the particle density, m is the particle mass, k is Boltzmann's constant, and T is the temperature. The current density at P is the result of integrating over only those trajectories that connect with the space plasma. To find whether a trajectory is acceptable, a particle is assumed to arrive at P with a given kinetic energy and set of impact angles θ_V and φ_V. The direction of the particle is reversed, and it is sent back away from P, either to end up in the space plasma or land elsewhere on the disk. If the particle lands elsewhere on the disk, the trajectory is not an allowed trajectory, since no particles are emitted by the disk (photoelectric effect and secondary emissions have been neglected). If the trajectory connects with the space plasma, it is allowed and contributes to the collected current density at P.

The particle moves along its path under the influence of the electrostatic field and of any magnetic field which may be present, according to the equation of motion

$$m \frac{d\vec{V}}{dt} = q (\vec{E} + \vec{V} \times \vec{B})$$

The trajectory is found by integrating this equation numerically, using the requirement

of energy conservation to adjust step size.

The electrostatic field was found by using the principle of superposition. Closed-form solutions exist for the voltage and the components of the electric field around a circular disk of uniform voltage. The solutions from several of these uniform voltage disks of different sizes are simply added together to get the solution for this problem where the voltage on the disk is not uniform (fig. 3). The voltage on each of these disks is chosen so that the total voltage from all disks gives the desired voltage distribution from the center of the pinhole to the outer edge of the insulation, that is, so that the boundary conditions are satisfied.

In practice, the voltage on the insulator is specified at the inner radius where the pinhole and insulation meet, at the outer radius, and at various points in between. A typical voltage profile is shown in figure 2, which is based on measurements by Boeing (ref. 6).

This superposition approach, together with the fact that long-range collective effects are not included, avoids the necessity for the finite difference approach used by Parker and Whipple (refs. 7 to 9).

The starting point for calculating the pinhole currents was the voltage profile shown in figure 2. This will be referred to as the "very positive" case because of the very high positive voltages over its surface. The pinhole had a radius of 0.19 centimeter and was at 10 000 volts. The radius of the dielectric was 5.1 centimeters. The computed voltage distribution in the space around the disk is shown in figure 4.

The electron and ion current densities j_e and j_i were computed at several points on the disk. The results are given in table I for temperatures $T = T_e = T_i$. (For high altitudes, the ion and electron temperatures are roughly equal.) The particle temperatures are expressed in terms of E_{th}, the random thermal kinetic energy of the particle. If the voltage profile shown in figure 2 had been the correct one for a disk with a perfect (no leakage) insulator, then the computed currents j_e and j_i would have been equal at each point on the insulator.

Instead, the electron current was everywhere too high relative to the ion current, which means that the voltage on the insulator was everywhere too positive. Figure 4 shows that the voltage is quite positive even far from the disk; this case, the "very positive case", represents an upper bound on the insulator voltage.

A discrepancy exists here because although this voltage profile is based on values obtained experimentally the calculations indicate that the insulation was too positive. A possible explanation lies in the fact that for the purpose of these calculations the insulation was assumed to have no leakage of current along the surface into the pinhole. As opposed to this ideal insulator, however, a real insulator could allow electrons to be drawn toward the very positive pinhole, preventing the buildup of negative charge and allowing the insulation to remain more positive than it would with no leakage.

This leakage could also explain the area effect, since now the total pinhole current would consist not only of current collected at the surface of the pinhole, but also the current that leaked in along the insulator. The additional current should increase roughly with the area of the insulation, which is in fact the case. Further evidence for this hypothesis is provided by the fact that an ideal insulator tends to mask the presence of the pinhole and reduce the collected current from its value with no surrounding insulation.

To test the effect on pinhole current of the voltage on the surrounding insulation, three other cases were considered - the slightly positive case, the slightly negative case, and the very negative case. These case names are descriptive of the voltages surrounding the disk. The voltage profiles are shown in figure 5, and the voltage contours in figures 6 to 8.

The electron current densities at the center of the pinhole are shown in table II(a) for each as $(j_e/j_{eo})(E_{th}/\psi_p)$, where ψ_p is the pinhole voltage (10 000 V in all cases). The ion current was negligible.

It is apparent from table II(a) that the current collected by a pinhole is strongly influenced by the voltage on the surrounding insulation. This is especially evident in the results of the slightly positive and slightly negative cases at low electron temperatures. If the presence of the pinhole can be felt even slightly by the electrons, considerable current will be collected. But, if the pinhole is masked by the presence of the negative insulation, the collected current is greatly reduced.

The importance of the masking effect of an ideal insulator on collected current was also shown in two other ways.

First, the effect of pinhole size was considered. The pinhole currents were calculated for the four cases using a 50 percent larger pinhole. These currents are shown in table II(b), and the voltage contours in figures 9 to 12. Comparison of the two positive cases for the two pinhole sizes shows that once the pinhole can be "seen", pinhole size does not have much effect on current density. Since the current density was fairly uniform across the pinhole surface, the total pinhole current in this case would be roughly proportional to pinhole area. Increasing the pinhole radius in the "slightly negative" case, however, resulted in a large increase in the current density. Comparison of the voltage contours in figures 7 and 11 shows that this can be explained by the fact that the pinhole voltage "punched through" the masking effect of the surrounding insulation.

In the second test the current was calculated for a 0.19-centimeter-radius 10-kilovolt circular electrode with no insulation surrounding it. The currents are shown in table III, along with the currents for the very positive case. The voltage contours are shown in figure 13. Comparing figures 4 and 13 shows that the presence of the insulator tends to reduce the voltage in the space surrounding the pinhole, and this reduction in voltage is reflected in a reduction in current collected by the pinhole (table III). This is

true even in the comparison made here, where the voltage profile used on the disk was too positive, as has been shown. Therefore, any area effect must be due to some mechanism not included in these calculations. As discussed earlier, the area effect is probably due to surface leakage on the surrounding insulation.

Even if some way is found to reduce this surface leakage, these results indicate that pinholes could still be a problem on satellites, where high-voltage surfaces would be covered by insulation. A small, isolated pinhole may not have significant leakage to the space plasma, but as micrometeorites cause other nearby pinholes, the masking effect of the insulation will be reduced, and the leakage current could increase rapidly because of the combined effects of increased current density and increased pinhole area.

For completeness, the effect of different pinhole voltages on the collected current was also considered. The results are shown in figure 14. To get the variation of current with voltage, all the voltages on the very positive case were divided by 10 (ψ_P = 1 kV) and then by 10 again (ψ_P = 100 V). The shape of the voltage contours is the same as that shown in figure 4, divided by 10 and 100. For $\psi_P >> E_{th}$

$$\frac{j_e}{j_{eo}} \frac{E_{th}}{\psi_P} \simeq \text{constant}$$

Since

$$j_{eo} = n_e q_e \left(\frac{kT_e}{2\pi m_e}\right)^{1/2} = n_e \left(\frac{q_e^3 E_{th}}{3\pi m_e}\right)^{1/2}$$

then

$$j_e \simeq (\text{constant}) \psi_P n_e \left(\frac{q_e^3}{3\pi m_e E_{th}}\right)^{1/2}$$

Hence, if the plasma temperature is much lower than the pinhole voltage, j_e is directly proportional to electron density and pinhole voltage and is inversely proportional to the square root of the plasma temperature. The inverse temperature dependence in this case is reasonable, as the current collecting surface will have a greater effect on electrons with less thermal energy, so that the current will increase as the temperature decreases.

On the other hand, if $E_{th} >> \psi_P$, $(j_e/j_{eo})(E_{th}/\psi_P)$ approaches the limit (E_{th}/ψ_P), or $j_e \approx j_{eo}$. This is to be expected, as the low voltage will have little effect on the energetic high-temperature electrons, and the current density will be just the random current density j_{eo}. Thus, the current calculation techniques used here give reasonable results for the variation of current with voltage.

CONCLUSIONS

A procedure using the trajectory tracing method of Parker and Whipple has been described for calculating the current collected from a dilute plasma through a pinhole defect in the insulation covering a high voltage surface. The geometrical model used is two concentric circular disks. The inner disk is at a constant potential and represents the pinhole. The region between the inner disk and the edge of the outer disk represents the surrounding insulation and is not at a uniform voltage.

Currents are calculated for cases where the voltage profile on the insulation is adjusted so the potential field surrounding the pinhole becomes either very positive, slightly positive, slightly negative, or very negative. The effect of pinhole size and pinhole voltage is also considered.

The results indicate that the large area of relatively negative insulation tends to mask the presence of the pinhole and that both the voltage in the space around the pinhole and the current collected by the pinhole are reduced by the presence of the insulation. This masking effect means that the "area" effect reported by some observers, in which the surrounding insulation increases pinhole current, cannot be explained solely by electrostatic effects. Instead, the results of this report indicate that the area effect is probably due to leakage of current along the insulation surface into the pinhole.

The masking effect is reduced as pinhole area is increased relative to the insulation area. This is likely to occur on satellites as micrometeorites puncture the insulation covering high-voltage surfaces. When this happens, all the pinholes could start to collect large currents.

Lewis Research Center,
National Aeronautics and Space Administration,
Cleveland, Ohio, February 5, 1975,
505-04.

APPENDIX A

METHOD OF SOLUTION

This appendix includes a detailed description of how the currents are calculated by the trajectory tracing technique and how the resulting integrals are evaluated. Also included are descriptions of how the particle trajectories are calculated and how the electrostatic field around the disk was calculated.

The normal current density at a point P on the disk whose position vector is $\vec{r}_p$ is

$$j(\vec{r}_p) = \int\int\int_{\text{allowed}} qf(\vec{r}_p, \vec{V})\vec{V} \cdot \hat{n}V^2 \, dV \sin\theta_V \, d\theta_V \, d\varphi_V \tag{A1}$$

where θ_V and φ_V give the direction of $\vec{V}$ at P (fig. 15). In equation (A1) "allowed" refers to the fact that only those particle trajectories that connect with the space plasma contribute to the current collected at P. If the current is being collected on the top side of the disk, the possible values for θ_V and φ_V are $0 \le \varphi_V \le 2\pi$ and $\pi/2 \le \theta_V \le \pi$.

The method for calculating the current makes use of the fact that f is a solution of Boltzmann's equation so that it has the same numerical value everywhere along a trajectory (refs. 7 to 9). Hence, it has the same value at P, at one end of the trajectory, as it did at its starting point in the space plasma, at the other end of the trajectory. This is true even in a magnetic field, as long as collisions can be ignored so that trajectories are curves of constant energy.

The distribution at "infinity" is taken to be Maxwell-Boltzmann and nonstreaming:

$$f(\vec{r}_p, \vec{V}) = n_o \left(\frac{m}{2\pi kT}\right)^{3/2} e^{-mV_\infty^2/2kT} = f(\vec{r}_\infty, \vec{V}_\infty) \tag{A2}$$

It is more convenient to work in terms of energies. Equation (A2) becomes

$$f(\vec{r}_p, E_{ke}) = f(\vec{r}_\infty, E_{ke\infty}) = n_o \left(\frac{3m}{4\pi|q|E_{th}}\right)^{3/2} e^{-3E_{ke\infty}/2E_{th}} \tag{A3}$$

where

$$\frac{1}{2} mV_{rms}^2 = \frac{3}{2} kT \equiv |q| E_{th} \tag{A4}$$

$$\frac{1}{2} mV^2 = |q| E_{ke}$$

The random current density in space j_o is the charge crossing a surface per unit area per unit time. For a Maxwell-Boltzmann distribution

$$j_o = qn_o \left(\frac{kT}{2\pi m}\right)^{1/2} \quad A/m^2 \tag{A5}$$

Since the collected currents will be written in terms of j_o, equation (A3) is rewritten as

$$f(\vec{r}_\infty, E_{ke\infty}) = \frac{9}{8\pi} \frac{j_o}{q} \left(\frac{m}{|q| E_{th}}\right)^2 e^{-3E_{ke\infty}/2E_{th}} \tag{A6}$$

Making use of the fact that energy is conserved along a trajectory gives

$$f(\vec{r}_p, E_{ke}) = \frac{9}{8\pi} \frac{j_o}{q} \left(\frac{m}{|q| E_{th}}\right)^2 e^{-3/2 \left\{\left[E_{ke} + (q/|q|)\psi(\vec{r}_p)\right]/E_{th}\right\}} \tag{A7}$$

where $\psi(\vec{r}_p)$ is the potential (in volts) at P and $(q/|q|)\psi(\vec{r}_p)$ is the potential energy (in eV) at P.

It is now possible to use equations (A1) and (A7) to calculate the current collected at P. First, however, note that

$$\vec{V} \cdot \hat{n} = \vec{V} \cdot -\hat{z} = -V \cos \theta_V$$

and that

$$V^3 \, dV = 2 \left(\frac{q}{m}\right)^2 E_{ke} \, dE_{ke}$$

It is also necessary to consider the allowed range of integration. For a given value of θ_V and φ_V, there will be a minimum kinetic energy below which no particles will be collected. From energy considerations alone, the minimum energy (in eV) of a particle collected by an attractive potential must be at least the voltage at the collection point. It could be zero for a repulsing potential. The minimum kinetic energy may still be higher than that allowed just on the basis of the voltage of the collection point. This may be seen by considering a particle ejected from the current collection point. If the particle is ejected with too low a kinetic energy, it will fall back somewhere else on the disk and not connect with the space plasma (fig. 16).

At a given point P on the disk, the minimum kinetic energy will depend on θ_V and φ_V. For instance, suppose the electron current collected at the center of the pinhole is being calculated and that the potential on the disk is everywhere positive (as in fig. 2). The minimum kinetic energy will be greater if θ_V is near $\pi/2$ than if θ_V is near π, because, to avoid being captured at some other point on the disk, an electron arriving on a trajectory that just grazes the surface will have to be going faster than one coming from straight above. Equation (A1) may now be written as

$$j(\vec{r}_p) = -j_o \frac{9}{4\pi E_{th}^2} \int_{\varphi_V=0}^{2\pi} \int_{\theta_V=\pi/2}^{\pi} \int_{E_{ke}=E_{min}(\theta_V, \varphi_V)}^{\infty} e^{-3/2\left\{\left[E_{ke} + (q/|q|)\psi(\vec{r}_p)\right]/E_{th}\right\}} \times E_{ke}\, dE_{ke} \cos\theta_V \sin\theta_V\, d\theta_V\, d\varphi_V \qquad (A8)$$

The integral over kinetic energy can be performed analytically by using the result

$$\int_b^{\infty} x e^{-ax}\, dx = \frac{e^{-ab}}{a^2}(ab + 1)$$

Then equation (A8) becomes

$$\frac{j(\vec{r}_p)}{j_o} = -\frac{1}{\pi} \int_0^{2\pi} \int_{\pi/2}^{\pi} \left[\frac{3}{2}\frac{E_{min}(\theta_V, \varphi_V)}{E_{th}} + 1\right] e^{-3/2\left\{\left[E_{min}(\theta_V, \varphi_V) + (q/|q|)\psi(\vec{r}_p)\right]/E_{th}\right\}} \times \sin\theta_V \cos\theta_V\, d\theta_V\, d\varphi_V \qquad (A9)$$

The integrations in equation (A9) must be performed numerically. No matter what

numerical integration scheme is chosen, it is necessary to know E_{min} for various values of θ_V and φ_V. The technique used here was weighted Gaussian quadratures, which works in the following way: The integral $\int_a^b f(x)\,dx$ is approximated by the sum

$$\sum_{i=1}^{N} w_i f(x_i)$$

where the w_i are weights assigned to these points and the x_i are various values of x in the range $a \le x \le b$. The values of w_i and x_i are found in handbooks (ref. 11) and depend on the length of the interval and on N, the number of points used in the approximation. Generally, Gaussian quadrature gives the best accuracy with the fewest values of the integrand. In this case it meant having to evaluate the fewest values of E_{min}. Each value of E_{min} required considerable computer time to evaluate.

To find E_{min} for a given value of θ_V and φ_V, consider a particle arriving at the current collection point P and having these impact angles. It will have some kinetic energy E_{ke} at impact. Since collisions are being ignored, the trajectory is dynamically reversible. The particle is sent back along the same path, starting at P with E_{ke}. The path will terminate either in the space plasma or somewhere on the disk. If the particle came from the plasma, $E_{ke} \ge E_{min}$, so the process is repeated with the same θ_V and φ_V and a smaller value of E_{ke} until the path terminates on the disk. Then $E_{ke} \le E_{min}$ (see fig. 16). The range between the upper and lower bounds on E_{min} is reduced until a sufficiently accurate value of E_{min} is found for this value of θ_V and φ_V. The criterion used here was that the difference between the upper and lower bounds was within 1 percent of the total energy. This is repeated for as many values of θ_V and φ_V as necessary to evaluate the integrals.

Unless there is a potential well surrounding the current collection point, there will be, for a given value of φ_V, a value θ_V above which the minimum kinetic energy (in eV) equals the potential at that point. Let this value of θ_V be called θ_2. For low plasma temperatures the exponential factor in equation (A9) will change rapidly from one for $\theta_V \ge \theta_2$ to zero for $\theta_V < \theta_2$. The change is less abrupt for higher plasma temperatures; nevertheless, Gaussian quadratures tend to give poor results for this step-function type of behavior.

Sufficient accuracy could be obtained by approximating the factor

$$g = \left(\frac{3}{2}\frac{E_{min}}{E_{th}} + 1\right)\exp\left(-\frac{3}{2}\frac{E_{min} + \frac{q}{|q|}\psi(\vec{r}_p)}{E_{th}}\right)$$

by a function that is zero for $\theta_V < \theta_1$, rises linearly from C_1 at θ_1 to $C_2 = (3/2)(\psi(\vec{r}_p)/E_{th}) + 1$ at $\theta_V = \theta_2$, and is equal to C_2 between θ_2 and π. This is shown in figure 17 where the current collection point is the center of the pinhole and where there is no φ dependence. The values of θ_1, θ_2, and C_1 depend on φ_V and E_{th}, and they are obtained by plotting g against θ_V for a given value of φ_V. Equation (A9) becomes

$$\frac{j}{j_o} = -\frac{1}{\pi}\int_0^{2\pi}\left\{\int_{\theta_1}^{\theta_2}\left[\frac{C_2 - C_1}{\theta_2 - \theta_1}(\theta - \theta_1) + C_1\right]\sin\theta\cos\theta\,d\theta + C_2\int_{\theta_2}^{\pi}\sin\theta\cos\theta\,d\theta\right\}d\varphi_V$$

$$= -\frac{1}{4\pi}\int_0^{2\pi}\left\{(C_2 - C_1)\left[\frac{\cos(\theta_2 + \theta_1)\sin(\theta_2 - \theta_1)}{\theta_2 - \theta_1} - 1\right] - 2C_1\sin^2\theta_1\right\}d\varphi_V$$

This integral is now in a form where Gaussian quadratures will give good results. For most of the calculations, however, the current collection point was the center of the pinhole, so the integration over φ_V was trivial.

The next thing to consider is how the particle trajectories are calculated. Lagrange's equations (ref. 12) for a particle moving in a conservative field are

$$\frac{d}{dt}\left(\frac{\partial L}{\partial \dot{q}_i}\right) - \frac{\partial L}{\partial q_i} = 0 \tag{A10}$$

where q_i is a generalized coordinate (not to be confused with charge on ions) and

$$\dot{q}_i = \frac{dq_i}{dt}$$

The Lagrangian for a charged particle in an electromagnetic field is

$$L = \frac{1}{2}mV^2 - q(\psi - \vec{V}\cdot\vec{A}) \tag{A11}$$

Provision is made for the possibility of a magnetic field, since originally the effect of a magnetic field on the current was to be included in the calculations.

Cylindrical coordinates are used with the disk in the $z = 0$ plane and the z-axis the axis of symmetry. In vector form the velocity $\vec{V}$ is

$$\vec{V} = \dot{\rho}\hat{\rho} + \rho\dot{\varphi}\,\hat{\varphi} + \dot{z}\hat{z} \tag{A12}$$

where $\hat{\rho}$, $\hat{\varphi}$, $\hat{z}$ are unit vectors in the ρ, φ, and z directions.

Equation (A11) becomes

$$L = \frac{m}{2}(\dot{\rho}^2 + \rho^2\dot{\varphi}^2 + \dot{z}^2) - q\left[\psi - (\dot{\rho}A_\rho + \rho\dot{\varphi}A_\varphi + \dot{z}A_z)\right] \tag{A13}$$

and (A10) becomes

$$\left.\begin{aligned}
\frac{d}{dt}(m\dot{\rho} + qA_\rho) &= m\rho\dot{\varphi}^2 + q\dot{\varphi}A_\varphi - q\left(\frac{\partial\psi}{\partial\rho} - \dot{\rho}\frac{\partial A_\rho}{\partial\rho} - \rho\dot{\varphi}\frac{\partial A_\varphi}{\partial\rho} - \dot{z}\frac{\partial A_z}{\partial\rho}\right)\\
\frac{d}{dt}(m\rho^2\dot{\varphi} + q\rho A_\varphi) &= q\left(-\frac{\partial\psi}{\partial\varphi} + \dot{\rho}\frac{\partial A_\rho}{\partial\varphi} + \rho\dot{\varphi}\frac{\partial A_\varphi}{\partial\varphi} + \dot{z}\frac{\partial A_z}{\partial\varphi}\right)\\
\frac{d}{dt}(m\dot{z} + qA_z) &= q\left(-\frac{\partial\psi}{\partial z} + \dot{\rho}\frac{\partial A_\rho}{\partial z} + \rho\dot{\varphi}\frac{\partial A_\varphi}{\partial z} + \dot{z}\frac{\partial A_z}{\partial z}\right)
\end{aligned}\right\} \tag{A14}$$

Equations (A14) can be written in terms of the components of the magnetic field $\vec{B}$ by the use of

$$\vec{B} = \nabla \times \vec{A} \tag{A15}$$

and

$$\frac{dA_c}{dt} = \frac{\partial A_c}{\partial t} + \dot{\rho}\frac{\partial A_c}{\partial\rho} + \dot{\varphi}\frac{\partial A_c}{\partial\varphi} + \dot{z}\frac{\partial A_c}{\partial z} \tag{A16}$$

where c stands for any of the components of $\vec{A}$.

In cylindrical coordinates equation (A15) is

$$\left.\begin{aligned}
B_\rho &= \frac{1}{\rho}\frac{\partial A_z}{\partial\varphi} - \frac{\partial A_\varphi}{\partial z}\\
B_\varphi &= \frac{\partial A_\rho}{\partial z} - \frac{\partial A_z}{\partial\rho}\\
B_z &= \frac{1}{\rho}\frac{\partial(\rho A_\varphi)}{\partial\rho} - \frac{1}{\rho}\frac{\partial A_\rho}{\partial\varphi}
\end{aligned}\right\} \tag{A17}$$

Using equations (A16) and (A17), equations (A14) become

$$m\ddot{\rho} = q\left(-\frac{\partial\psi}{\partial\rho} - \frac{\partial A_\rho}{\partial t}\right) + m\rho\dot{\varphi}^2 + q\left[\rho\dot{\varphi}\left(\frac{\partial A_\varphi}{\partial\rho} + \frac{1}{\rho}A_\varphi - \frac{1}{\rho}\frac{\partial A_\rho}{\partial\rho}\right) - \dot{z}\left(\frac{\partial A_\rho}{\partial z} - \frac{\partial A_z}{\partial\rho}\right)\right]$$

$$\frac{d}{dt}(m\rho^2\dot{\varphi}) = q\left(-\frac{\partial\psi}{\partial\varphi} - \rho\frac{\partial A_\varphi}{\partial t}\right) + q\left[\dot{z}\left(\frac{\partial A_z}{\partial\varphi} - \rho\frac{\partial A_\varphi}{\partial z}\right) - \dot{\rho}\left(A_\varphi + \rho\frac{\partial A_\varphi}{\partial\rho} - \frac{\partial A_\rho}{\partial\varphi}\right)\right]$$

$$m\ddot{z} = q\left(-\frac{\partial\psi}{\partial z} - \frac{\partial A_z}{\partial t}\right) + q\left[\dot{\rho}\left(\frac{\partial A_\rho}{\partial z} - \frac{\partial A_z}{\partial\rho}\right) - \rho\dot{\varphi}\left(\frac{1}{\rho}\frac{\partial A_z}{\partial\varphi} - \frac{\partial A_\varphi}{\partial z}\right)\right]$$

or

$$m\ddot{\rho} = m\rho\dot{\varphi}^2 + qE_\rho + q(\rho\dot{\varphi}B_z - \dot{z}B_\varphi) \tag{A18(a)}$$

$$\frac{d}{dt}(m\rho^2\dot{\varphi}) = q\rho E_\varphi + q\rho(\dot{z}B_\rho - \dot{\rho}B_z) \tag{A18(b)}$$

$$m\ddot{z} = qE_z + q(\dot{\rho}B_\varphi - \rho\dot{\varphi}B_\rho) \tag{A18(c)}$$

Note that E_φ is zero because of symmetry; therefore, in the absence of a magnetic field, equation (A18(b)) is $d/dt(m\rho^2\dot{\varphi}) = 0$, which is the statement of conservation of angular momentum. If there is no explicit time dependence, $\vec{E} = -\nabla\psi$, and the equations of motion are

$$\left.\begin{aligned} m\ddot{\rho} &= m\rho\dot{\varphi}^2 - q\frac{\partial\psi}{\partial\rho} + q(\rho\dot{\varphi}B_z - \dot{z}B_\varphi) \\ m\ddot{\varphi} &= -\frac{2m\dot{\rho}\dot{\varphi}}{\rho} + q\left(\frac{\dot{z}}{\rho}B_\rho - \frac{\dot{\rho}}{\rho}B_z\right) \\ m\ddot{z} &= -q\frac{\partial\psi}{\partial z} + q(\dot{\rho}B_\varphi - \rho\dot{\varphi}B_\rho) \end{aligned}\right\} \tag{A19}$$

If the gradient of ψ and the components of $\vec{B}$ are known everywhere, the trajectory of an incoming ion or electron can be reconstructed in the following manner. Let the particle land at time $t = 0$. First, the incoming direction of the particle is reversed so that it will travel backwards over the same path. (It is also necessary to re-

verse the direction of $\vec{B}$ at each point). Next, the position of the particle at a small time Δt earlier is found. If Δt is small enough, the new coordinates are approximately

$$\left.\begin{aligned} \rho_n &\simeq \rho + \dot{\rho}\,\Delta t + \frac{1}{2}\ddot{\rho}(\Delta t)^2 \\ \varphi_n &\simeq \varphi + \dot{\varphi}\,\Delta t + \frac{1}{2}\ddot{\varphi}(\Delta t)^2 \\ z_n &\simeq z + \dot{z}\,\Delta t + \frac{1}{2}\ddot{z}(\Delta t)^2 \end{aligned}\right\} \tag{A20}$$

The initial coordinates ρ, φ, and z are the coordinates of the current collection point. The initial velocities $\dot{\rho}$, $\dot{\varphi}$, and $\dot{z}$ are calculated from the kinetic energy at impact, E_{ke}, and from the impact angles θ_V and φ_V. The accelerations $\ddot{\rho}$, $\ddot{\varphi}$, and $\ddot{z}$ are found by using equations (A19) and the values of $\vec{E}$ and $\vec{B}$ at the current collection point. The new velocities are needed before the process can be repeated. These are

$$\left.\begin{aligned} \dot{\rho}_n &\simeq \dot{\rho} + \ddot{\rho}\,\Delta t \\ \dot{\varphi}_n &\simeq \dot{\varphi} + \ddot{\varphi}\,\Delta t \\ \dot{z}_n &\simeq \dot{z} + \ddot{z}\,\Delta t \end{aligned}\right\} \tag{A21}$$

The next point is found in the same fashion, with the position and velocity from equations (A20) and (A21) used as starting values. The particle is traced step by step back along its trajectory to its starting point, either in the space plasma or elsewhere on the disk. As a check on the size of Δt at each step, the kinetic energy at each point is calculated from the velocities and compared with the kinetic energy calculated from the initial energy of the particle and the potential at that point. The size of Δt was reduced until the agreement was within 0.3 percent. This technique has the added advantage of making the step size smaller where the field gradients and accelerations are larger. This maintains accuracy without wasting computer time.

The magnetic field can be chosen to represent the field of the Earth or the field of some electrical device on the satellite. The only requirement on the magnetic field is that it satisfy the relation $\nabla \cdot \vec{B} = 0$ to be physically realizable.

That leaves only the matter of calculating the electric field due to the disk. The finite difference approach used by Parker and Whipple was avoided by superposing the

potential and electric field due to several disks, each of which was at a uniform voltage (fig. 3).

The voltage around a disk of radius a and uniform voltage ψ_o is given in oblate spheroidal coordinates by Moon and Spencer (ref. 13):

$$\psi_1 = \frac{2}{\pi} \psi_o \cot^{-1}(\sinh \eta) \tag{A22}$$

Cylindrical and oblate spheroidal coordinates are related by

$$\left.\begin{aligned} \rho &= a \cosh \eta \sin \theta \\ \varphi &= \varphi \\ z &= a \sinh \eta \cos \theta \end{aligned}\right\} \tag{A23}$$

The inverse transformations are given by

$$\left.\begin{aligned} \cosh \eta &= \frac{1}{2a}\left[\sqrt{(\rho + a)^2 + z^2} + \sqrt{(\rho - a)^2 + z^2}\right] \\ \varphi &= \varphi \\ \sin \theta &= \frac{1}{2a}\left[\sqrt{(\rho + a)^2 + z^2} - \sqrt{(\rho - a)^2 + z^2}\right] \end{aligned}\right\} \tag{A24}$$

The parameter a enters in the following way: surfaces of constant η are oblate spheroids; the oblate spheroid for $\eta = 0$ reduces to a disk of radius a. Since there is no built-in inverse contangent function on the computer, it is convenient to rewrite equation (A22). Let $\tau = (\pi/2)(\psi_1/\psi_o)$ and $\beta = \sinh \eta$ so that $\beta = \cot \tau$ which gives

$$\tau = \sin^{-1} \frac{1}{\sqrt{1 + \beta^2}}$$

Substituting for τ and β,

$$\psi_1 = \frac{2}{\pi}\psi_o \sin^{-1}\frac{1}{\sqrt{1+\sinh^2\eta}}$$

$$= \frac{2}{\pi}\psi_o \sin^{-1}\frac{1}{\cosh\eta}$$

From equation (A24)

$$\psi_1(\rho, z) = \frac{2}{\pi}\psi_o \sin^{-1}\left[\frac{2a}{\sqrt{(\rho+a)^2+z^2}+\sqrt{(\rho-a)^2+z^2}}\right] \tag{A25}$$

Equation (A25) gives the voltage distribution about a single disk of radius a and voltage ψ_o. The principle of superposition is used to construct a solution that represents a pinhole surrounded by insulation (fig. 2). To see how this is done, consider the voltage at $z = 0$. From equation (A25)

$$\psi_1(\rho > a,\ z = 0) = \frac{2}{\pi}\psi_o \sin^{-1}\left(\frac{a}{\rho}\right) \tag{A26}$$

$$\psi_1(\rho \le a,\ z = 0) = \psi_o \tag{A27}$$

For the purpose of illustrating how the solution is obtained, suppose that pinhole-insulation system is to have the distribution given by having the three points $\rho = r_o(1),\ r_o(2),\ r_o(3)$ at the voltages $V_o(1),\ V_o(2),\ V_o(3)$. From equations (A25) to (A27), the general solution is

$$\psi(\rho, z) = \frac{2}{\pi}\sum_{i=1}^{3} V_b(i) \sin^{-1}\left\{\frac{2r_o(i)}{\sqrt{\left[\rho + r_o(i)\right]^2+z^2}+\sqrt{\left[\rho - r_o(i)\right]^2+z^2}}\right\} \tag{A28}$$

where the numbers $V_b(i)$ are the superposition voltages and satisfy the equations

$$\left.\begin{aligned} V_o(1) &= V_b(1) + V_b(2) + V_b(3) \\ V_o(2) &= \frac{2}{\pi} V_b(1) \sin^{-1} \frac{r_o(1)}{r_o(2)} + V_b(2) + V_b(3) \\ V_o(3) &= \frac{2}{\pi} V_b(1) \sin^{-1} \frac{r_o(1)}{r_o(3)} + \frac{2}{\pi} V_b(2) \sin^{-1} \frac{r_o(2)}{r_o(3)} + V_b(3) \end{aligned}\right\} \tag{A29}$$

The solution given in (A28) is generated by superimposing the voltages of three disks of radii $r_o(1)$, $r_o(2)$, and $r_o(3)$, having, respectively, the constant voltages $V_b(1)$, $V_b(2)$, and $V_b(3)$. On the $z = 0$ plane, $\psi(\rho, z=0)$ automatically reduces to

$$\left.\begin{aligned} \psi\left[\rho < r_o(1), 0\right] &= V_o(1) \\ \psi\left[\rho = r_o(2), 0\right] &= V_o(2) \\ \psi\left[\rho = r_o(3), 0\right] &= V_o(3) \end{aligned}\right\} \tag{A30}$$

The pinhole has radius $r_o(1)$ and voltage $V_o(1)$. The region between $r_o(1)$ and $r_o(3)$ is the insulation. In practice, equations (A29) are inverted numerically to get the numbers V_b, and these are retained in the memory of the computer. The voltage is calculated at each point where it is desired by using equation (A28).

The components of the electric field are still needed. The total electric field is calculated by adding the contributions due to individual constant voltage disks, as in calculating the potential. This can be seen by using the definition $\vec{E} = -\nabla\psi$, where ψ is given by equation (A28). The expressions for $E_{\rho 1}$ and E_{z1}, the ρ- and z-components of the electric field for a single disk of radius a and voltage V, are most easily obtained by converting from oblate spheroidal to cylindrical coordinates.

The electric field for a single disk expressed in oblate spheroidal coordinates is

$$\vec{E} = \frac{2}{\pi} \frac{\psi_o}{a} \hat{\eta} \frac{1}{\cosh \eta \sqrt{\cosh^2 \eta - \sin^2 \theta}} \tag{A31}$$

where $\hat{\eta}$ is the unit vector in the direction of increasing η. Let $\vec{e}_\eta$ be defined by

$$\hat{\eta} = \frac{\vec{e}_\eta}{\sqrt{\vec{e}_\eta \cdot \vec{e}_\eta}} \tag{A32}$$

The vector $\vec{e}_\eta$ is parallel to $\hat{\eta}$ but is not necessarily a unit vector. It is related to the unit vectors in cylindrical coordinates (ref. 14, p. 120) by

$$\vec{e}_\eta = \frac{\partial \rho}{\partial \eta}\hat{\rho} + \frac{\partial z}{\partial \eta}\hat{z} + \frac{\partial \varphi}{\partial \eta}\hat{\varphi} \tag{A33}$$

From equation (A23)

$$\vec{e}_\eta = a \sinh \eta \sin \theta \hat{\rho} + a \cosh \eta \cos \theta \hat{z} \tag{A34}$$

$$\vec{e}_\eta \cdot \vec{e}_\eta = a^2(\sinh^2 \eta \sin^2 \theta + \cosh^2 \eta \cos^2 \theta)$$

$$= a^2\left[(\cosh^2 \eta - 1)\sin^2 \theta + \cosh^2 \eta \cos^2 \theta\right]$$

$$= a^2(\cosh^2 \eta - \sin^2 \theta)$$

so that the unit vector $\hat{\eta}$ is

$$\hat{\eta} = \frac{1}{\sqrt{\cosh^2 \eta - \sin^2 \theta}}(\sinh \eta \sin \theta \hat{\rho} + \cosh \eta \cos \theta \hat{z})$$

From equation (A31), the components of the electric field are

$$\left.\begin{aligned} E_\rho &= \frac{2}{\pi}\frac{\psi_o}{a}\frac{\sinh \eta \sin \theta}{\cosh \eta(\cosh^2 \eta - \sin^2 \theta)} \\ E_z &= \frac{2}{\pi}\frac{\psi_o}{a}\frac{\cos \theta}{\cosh^2 \eta - \sin^2 \theta} \end{aligned}\right\} \tag{A36}$$

To get an expression in cylindrical coordinates, first use the relation

$$\cosh^2\eta - \sin^2\theta = \frac{1}{a^2}\left[\sqrt{(\rho + a)^2 + z^2}\sqrt{(\rho - a)^2 + z^2}\right] \tag{A37}$$

and then

$$E_\rho = \frac{2\psi_o a}{\pi}\frac{\sinh\eta \sin\theta}{\cosh\eta}\frac{1}{\left[\sqrt{(\rho + a)^2 + z^2}\sqrt{(\rho - a)^2 + z^2}\right]}$$

and

$$E_z = \frac{2\psi_o a}{\pi}\cos\theta\frac{1}{\left[\sqrt{(\rho + a)^2 + z^2}\sqrt{(\rho - a)^2 + z^2}\right]}$$

Equation (A24) supplies the expressions for $\cosh\eta$ and $\sin\theta$, and

$$\sinh\eta = \sqrt{\cosh^2\eta - 1}$$

and

$$\cos\theta = \sqrt{1 - \sin^2\theta}$$

APPENDIX B

SYMBOLS

$\vec{A}$	magnetic vector potential, V-sec/m
$\vec{B}$	magnetic field, Wb/m^2
C_1, C_2	parameters used in approximating integral in eq. (A9)
$\vec{E}$	electric field, V/m
E_{ke}	kinetic energy of particle arriving at current collection point, eV
$E_{ke\infty}$	kinetic energy of particle in undisturbed plasma, eV
E_{min}	minimum kinetic energy of particle arriving at current collection point, eV
E_{th}	thermal energy of particles in undisturbed plasma, eV
E_{z1}	z component of electric field about uniform potential disk
$E_{\rho 1}$	ρ component of electric field about uniform potential disk
$\vec{e}_\eta$	vector in η direction
f	distribution function, $(A/m^2)/(m/sec)^4$
$j(\vec{r}_p)$	normal current density at current collection point, A/m^2
j_e	normal electron current density, A/m^2
j_{eo}	electron current density in undisturbed plasma, A/m^2
j_i	normal ion current density, A/m^2
j_{io}	ion current density in undisturbed plasma, A/m^2
k	Boltzmann constant, J/K
L	Lagrangian function, J
m	particle mass, kg
m_e	electron mass, kg
$\hat{n}$	unit normal at current collection point
n_e	electron density in undisturbed plasma, m^{-3}
n_o	particle density in undisturbed plasma, m^{-3}
P	current collection point
q	charge on particle, C

q_e charge on electron, C

q_i i^{th} generalized coordinate in Lagrangian function

$\vec{r}_p$ position vector of current collection point

$r_o(i)$ points at which potential is specified for nonequipotential disk

T temperature, K

T_e electron temperature, K

T_i ion temperature, K

$\vec{V}$ particle velocity, m/sec

$V_b(i)$ superposition voltages for nonequipotential disk, V

$V_o(i)$ specified voltages on nonequipotential disk, V

$\vec{V}_\infty$ particle velocity in undisturbed plasma, m/sec

η, θ, φ coordinates in oblate spheroidal coordinate system

$\hat{\eta}$ unit normal in η direction

θ_V, φ_V angles that specify direction of incoming particle at current collection point (see fig. 15)

ρ, φ, z coordinates in cylindrical coordinate system

$\hat{\rho}, \hat{\varphi}, \hat{z}$ unit vectors in ρ, φ, and z directions

$\psi(\rho, z)$ electrostatic potential, V

ψ_P electrostatic potential on pinhole, V

ψ_o uniform potential, V

$\psi_1(\rho, z)$ electrostatic potential due to single disk at ψ_o, V

REFERENCES

1. Knauer, W.; Bayless, J. R.; Todd, G. T.; and Ward, J. W.: High Voltage Solar Array Study. (Hughes Research Labs.; NAS3-11535.) NASA CR-72675, 1970.

2. Springgate, W. F.; and Omen, Henry: High Voltage Solar Array Study. (D2-121734-1, Boeing Co.; NAS3-11534.) NASA CR-72674, 1969.

3. Cole, Robert K.; Ogawa, H. S.; and Sellan, J. M., Jr.: Operation of Solar Cell Arrays in Dilute Streaming Plasmas. (TRW-09357-6006-R000, TRW Systems; NAS3-10612.), NASA CR-72376, 1968.

4. Grier, N. T.; and McKinzie, D. J., Jr.: Current Drainage to a High Voltage Probe in a Dilute Plasma. AIAA Paper 72-105, Jan. 1972.

5. Bayless, J. R.; Herron, B. G.; and Worden, J. D.: High Voltage Solar Array Technology. AIAA Paper 72-443, Apr. 1972.

6. Kennerud, K. L.: High Voltage Solar Array Experiments. (Boeing Aerospace Co.; NAS3-14364.), NASA CR-121280, 1974.

7. Parker, Lee W.; and Whipple, Elden C., Jr.: Theory of a Satellite Electrostatic Probe. Annals of Physics, vol. 44, no. 1, Aug. 1967, pp. 126-161.

8. Whipple, Elden C., Jr.; and Parker, Lee W.: Theory of an Electron Trap on a Charged Spacecraft. J. Geophysical Research, vol. 74, no. 11, June 1969, pp. 2962-2971.

9. Whipple, Elden C., Jr.; and Parker, Lee W.: Effects of Secondary Electron Emission on Electron Trap Measurements in the Magnetosphere and Solar Wind. J. Geophysical Research, vol. 74, no. 24, Nov. 1969, pp. 5763-5774.

10. Stevens, N. John: Solar Array Experiments on the Sphinx Satellite. Paper presented at the 10^{th} Photovoltaic Specialists Conf., Palo Alto, Calif., Nov. 13-15, 1973.

11. Abramowitz, Milton; and Stegun, Irene A., eds.: Handbook of Mathematical Functions With Formulas, Graphs, and Mathematical Tables. Dover Publishing Co., 1964.

12. Goldstein, Herbert: Mechanics. Addison-Wesley Publishing Co., 1950.

13. Moon, Parry; and Spencer, Domina E.: Field Theory for Engineers. D. Van Nostrand Co., 1961.

14. Sokolnikoff, I. S.: Tensor Analysis, Theory and Applications to Geometry and Mechanics of Continua. Second ed., Wiley, 1964.

TABLE I. - ION AND ELECTRON CURRENT DENSITIES AT VARIOUS LOCATIONS ON INSULATOR - VERY POSITIVE CASE

Thermal energy, E_{th}, eV	Distance along radius, cm	Voltage at that point, $\psi(\vec{r}_p)$, V	Electron current density, j_e, A/m^2	Ion current density, j_i, A/m^2
0.1	1.7	375	1.18×10^{-2}	0
1	↓	↓	3.74×10^{-3}	0
10			1.20×10^{-3}	2.4×10^{-33}
100			4.39×10^{-4}	4.7×10^{-8}
0.1	2.7	225	7.20×10^{-3}	0
1	↓	↓	2.28×10^{-3}	0
10			7.39×10^{-4}	8.7×10^{-22}
100			2.95×10^{-4}	6.7×10^{-8}
0.1	3.8	125	4.10×10^{-3}	0
1	↓	↓	1.30×10^{-3}	0
10			4.32×10^{-4}	3.1×10^{-15}
100			1.99×10^{-4}	3.0×10^{-7}
0.1	4.8	75	2.41×10^{-3}	0
1	↓	↓	7.68×10^{-4}	3.1×10^{-57}
10			2.62×10^{-4}	7.1×10^{-12}
100			1.44×10^{-4}	6.5×10^{-7}
0.1	5.1	40	1.55×10^{-3}	0
1	↓	↓	4.97×10^{-4}	9.0×10^{-57}
10			1.80×10^{-4}	1.2×10^{-11}
100			1.30×10^{-4}	1.9×10^{-6}

TABLE II. - DIMENSIONLESS COLLECTED ELECTRON CURRENT AT CENTER OF PINHOLE, WITH INSULATION ADJUSTED TO PRODUCE VARIOUS VOLTAGE DISTRIBUTIONS AROUND DISK

[Disk radius, 5.1 cm.]

(a) Pinhole radius, 0.19 cm

Thermal energy, E_{th}, eV	Disk voltage distribution			
	Very positive	Slightly positive	Slightly negative	Very negative
	Collected dimensionless electron current, $(j_e/j_{eo})(E_{th}/\psi_p)$			
0.1	1.06	0.456	3×10^{-10}	0
1	1.06	.537	3×10^{-2}	1×10^{-34}
10	1.06	.762	0.45	6×10^{-5}
100	1.07	.974	.9	0.3
1000	1.27	1.09	1.2	1.06

(b) Pinhole radius, 0.285 cm

Thermal energy, E_{th}, eV	Disk voltage distribution			
	Very positive	Slightly positive	Slightly negative	Very negative
	Collected dimensionless electron current, $(j_e/j_{eo})(E_{th}/\psi_p)$			
0.1	1.09	1.07	0.749	0
1	1.09	1.08	.778	8×10^{-26}
10	1.09	1.08	.950	7×10^{-4}
100	1.11	1.09	1.07	0.4
1000	1.23	1.21	1.22	1.13

TABLE III. - EFFECT OF INSULATION ON PINHOLE CURRENT

Thermal energy, E_{th}, eV	10-kV, 0.19-cm circular disk with no insulation	10-kV, 0.19-cm circular disk plus insulation (very pos. case)
	Collected dimensionless electron current, $(j_e/j_{eo})(E_{th}/\psi_p)$	
0.1	1.41	1.06
1	1.41	1.06
10	1.41	1.06
100	1.42	1.07
1000	1.50	1.27

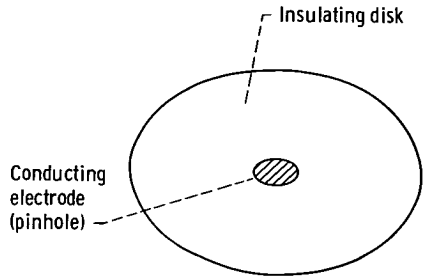

Figure 1. - Disk model.

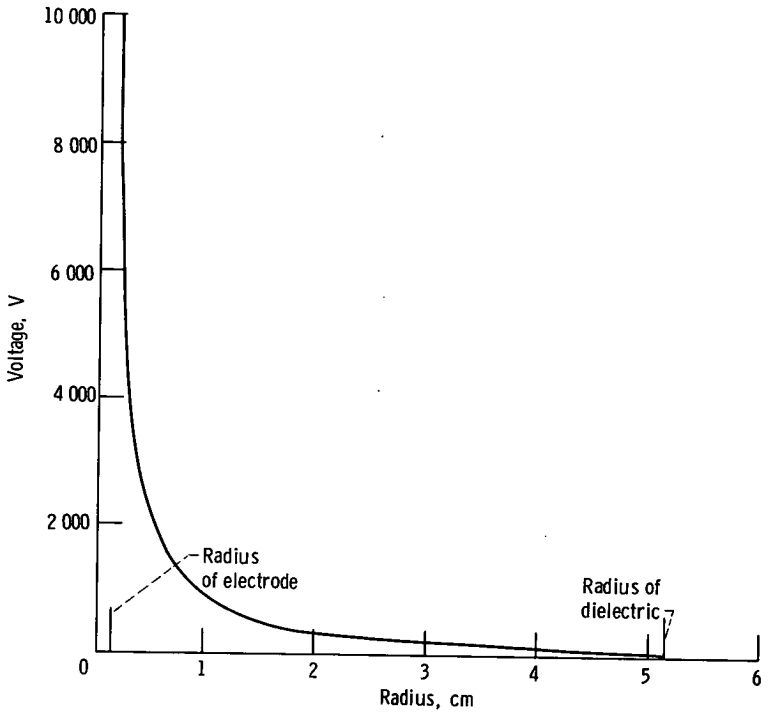

Figure 2. - Typical disk voltage profile.

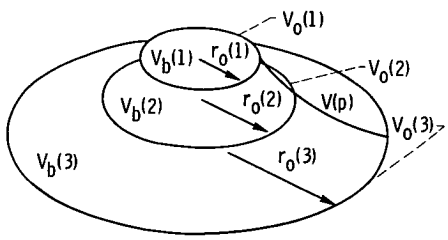

Figure 3. - Superposition of voltages from three disks of radii $r_o(1)$, $r_o(2)$, $r_o(3)$ and voltages $V_b(1)$, $V_b(2)$, $V_b(3)$ to give V(p), which has the values $V_o(1)$ at points $\leq r_o(1)$, $V_o(2)$ at $r_o(2)$, and $V_o(3)$ at $r_o(3)$.

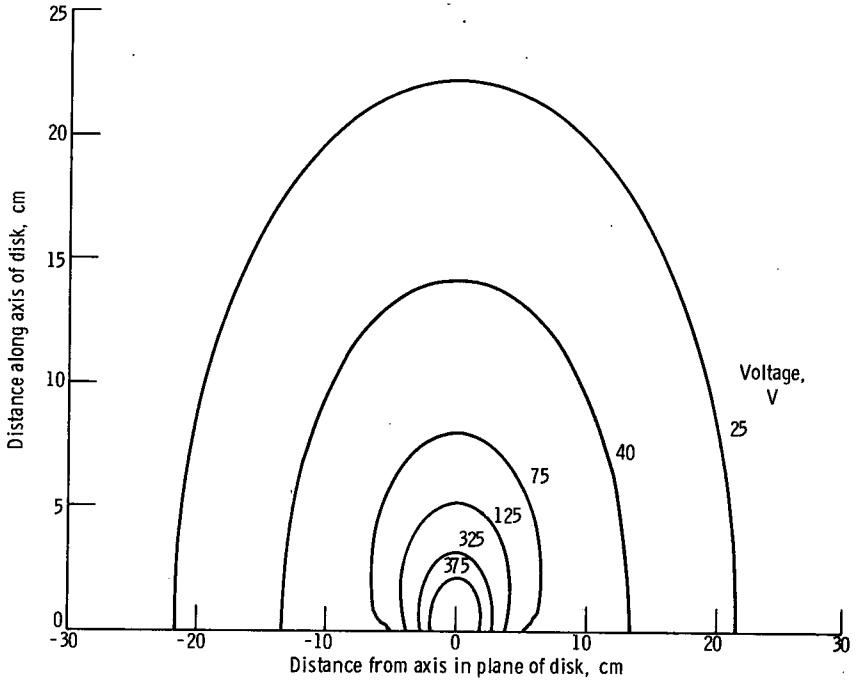

Figure 4. - Contours for very positive case; small pinhole.

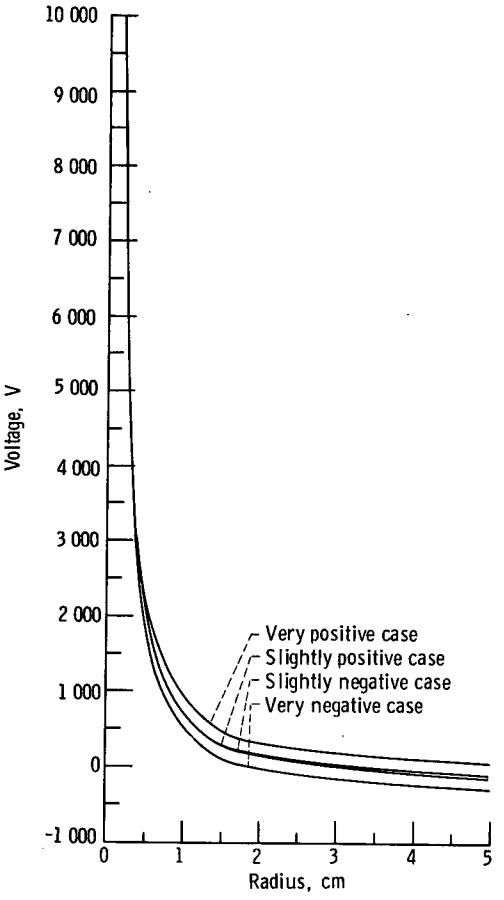

Figure 5. - Voltage profiles for various current collection cases; small pinhole.

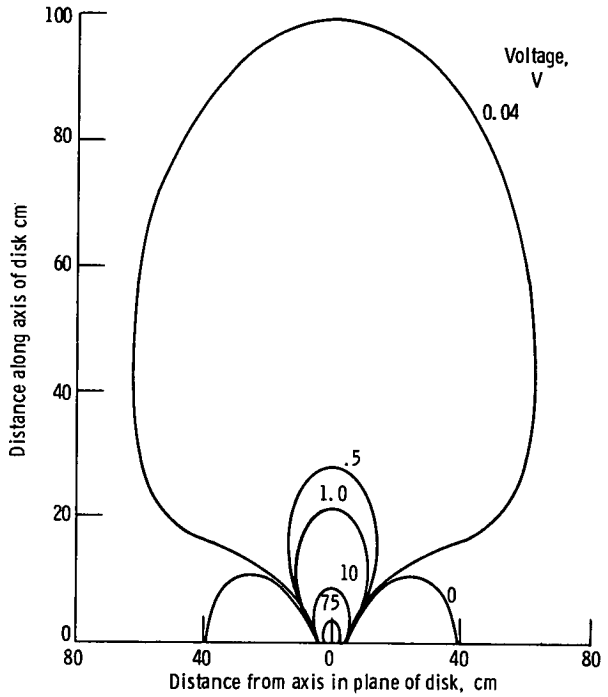

Figure 6. - Contours for slightly positive case; small pinhole.

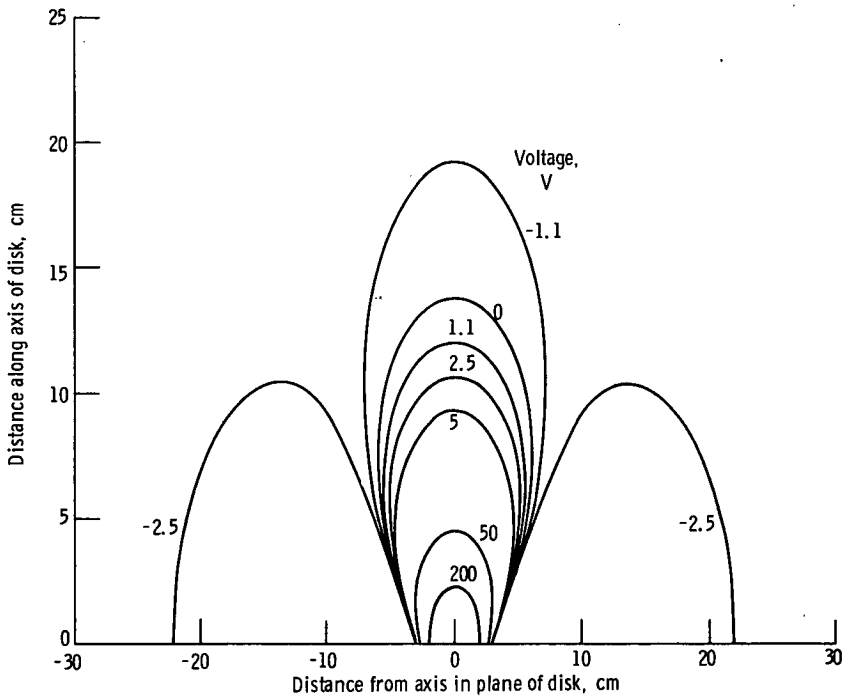

Figure 7. - Contours for slightly negative case; small pinhole.

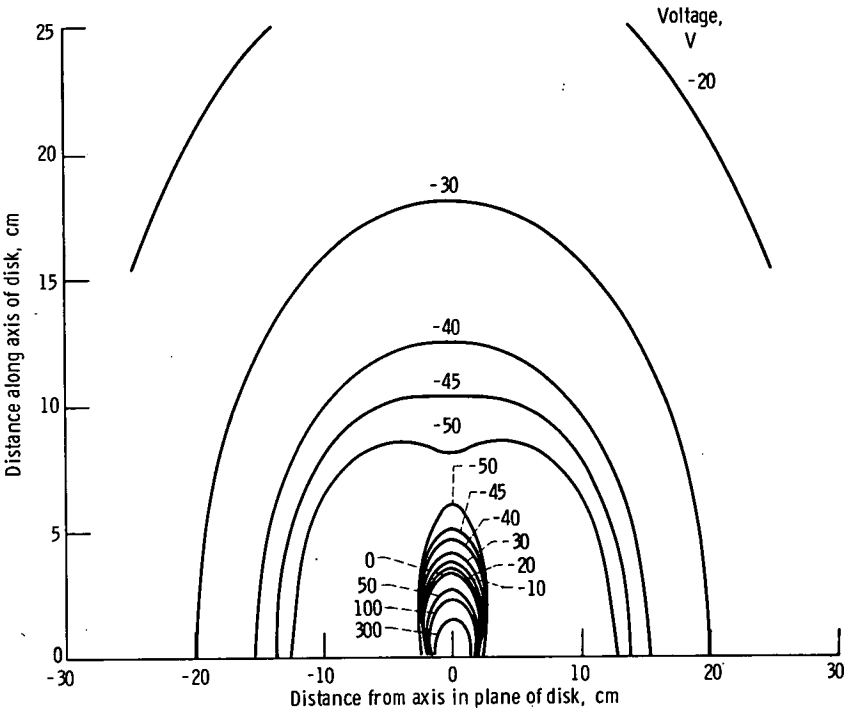

Figure 8. - Contours for very negative case; small pinhole.

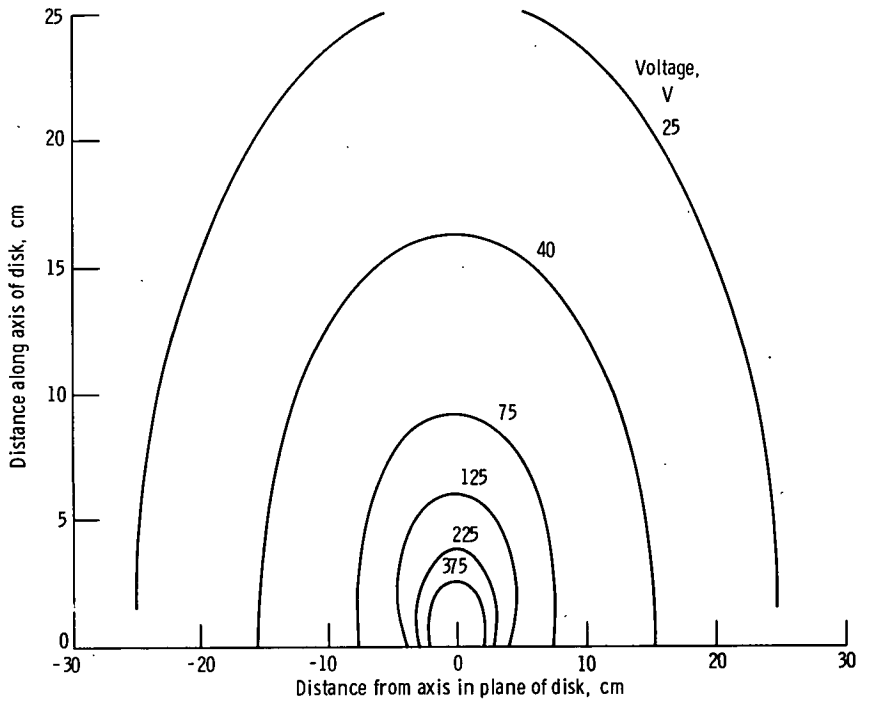

Figure 9. - Contours for very positive case; large pinhole.

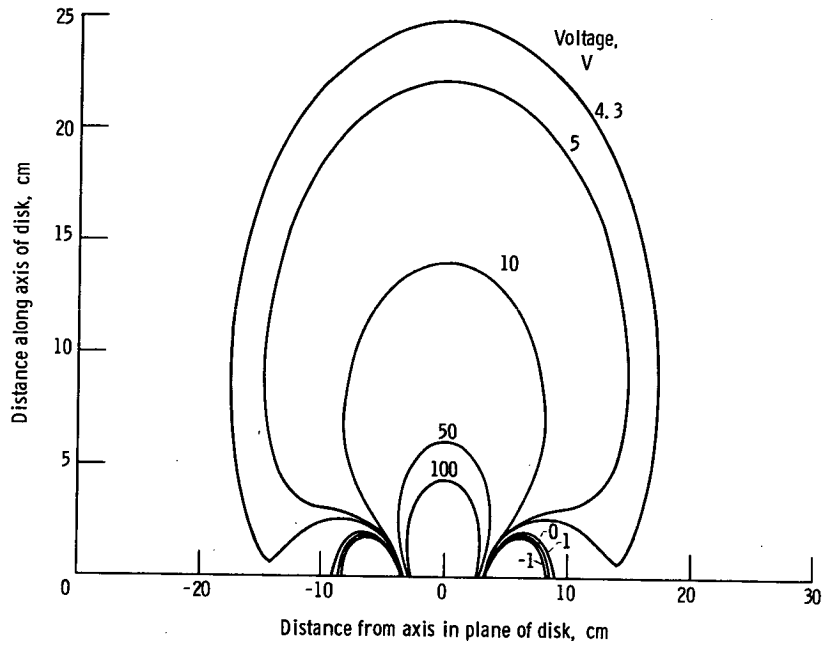

Figure 10. - Contours for slightly positive case; large pinhole.

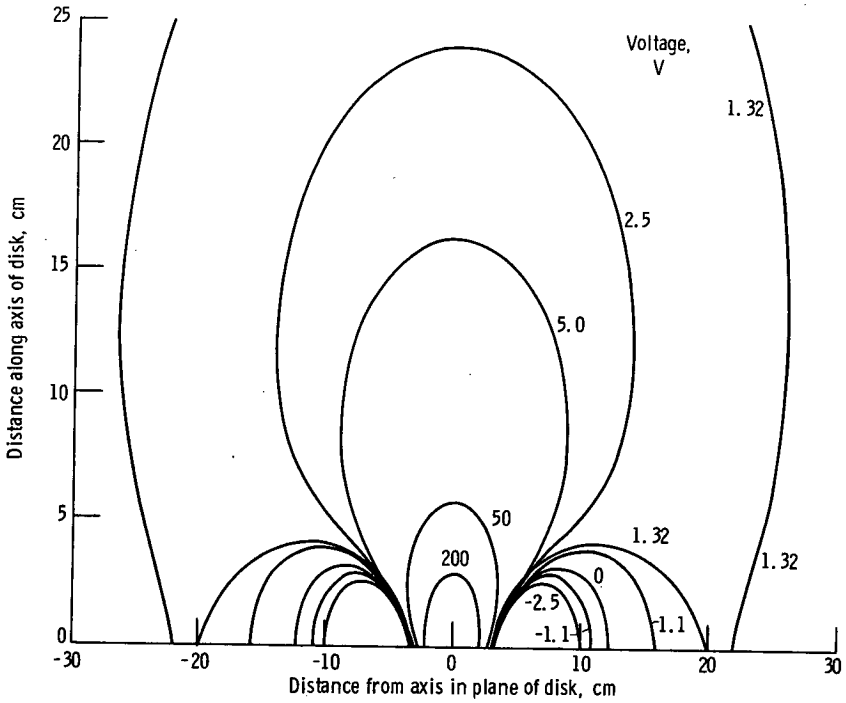

Figure 11. - Contours for slightly negative case; large pinhole.

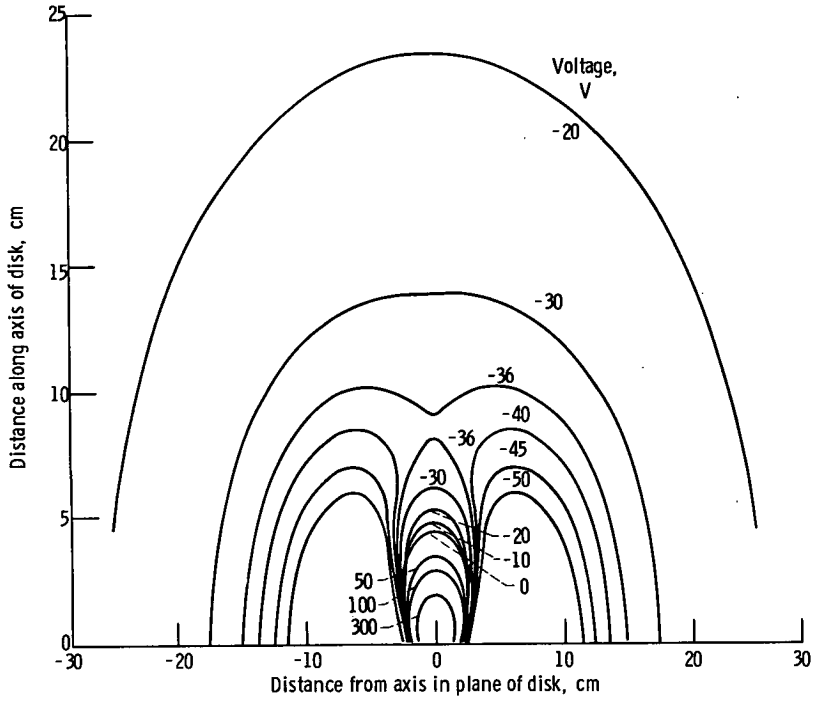

Figure 12. - Contours for very negative case; large pinhole.

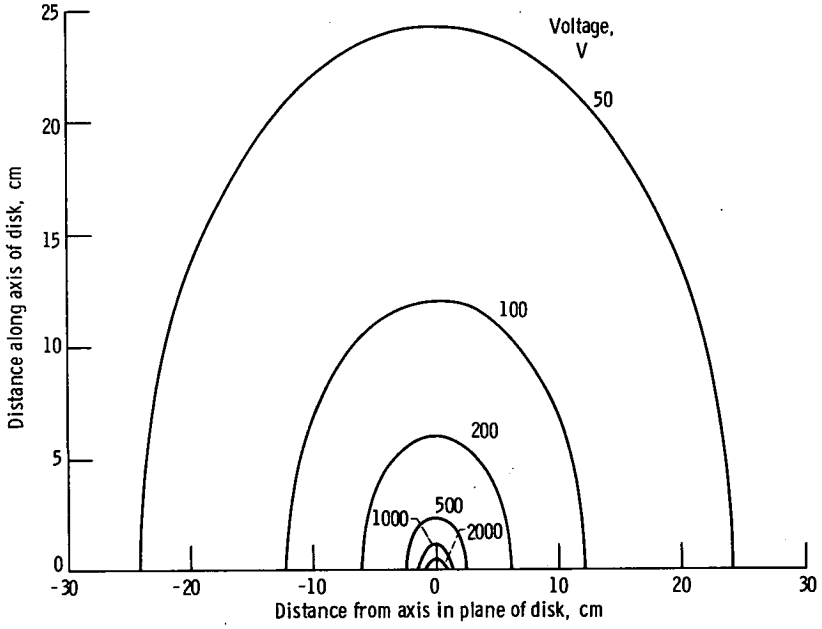

Figure 13. - Contours for 10 000-volt, 0.19-centimeter radius disk.

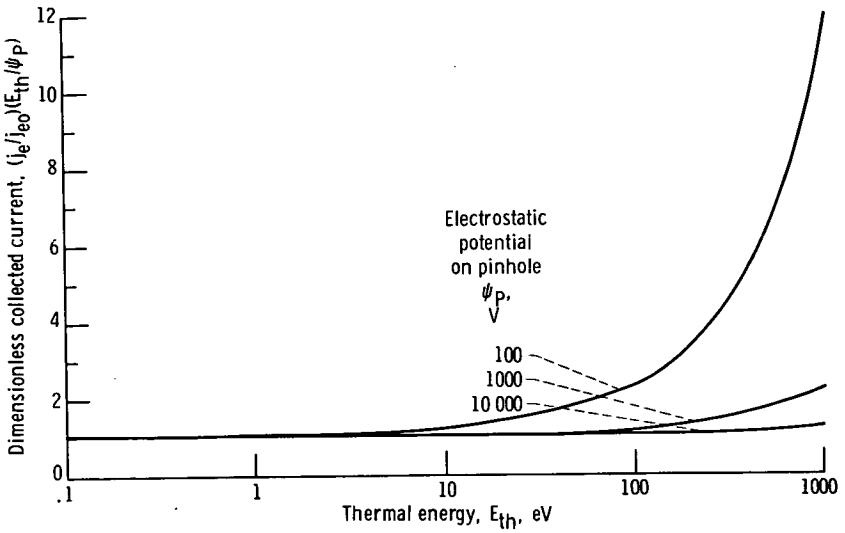

Figure 14. - Collected current density at center pf pinhole. Very positive case, small pinhole.

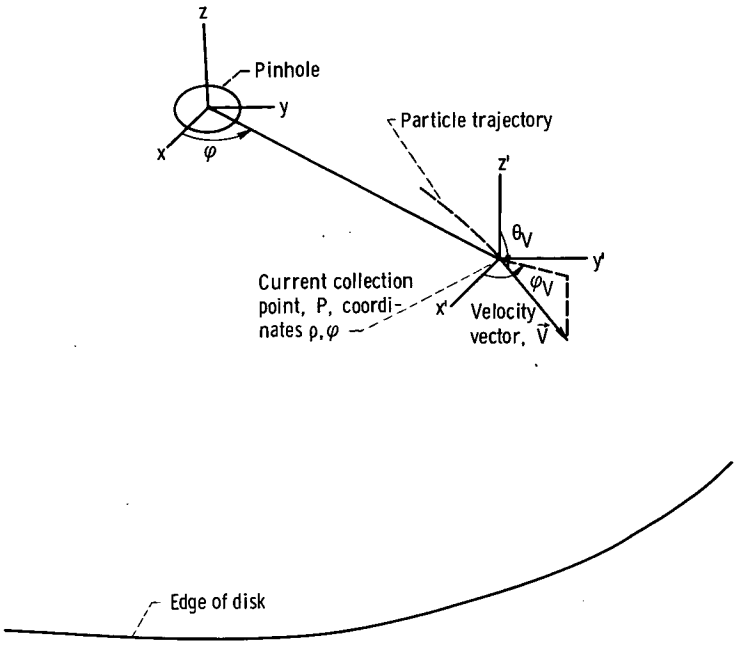

Figure 15. - Coordinates of current collection point and impact angles of trajectory.

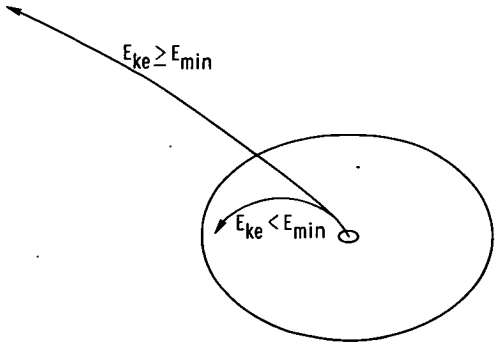

Figure 16. - Two trajectories having same impact angles at current collection point, but different kinetic energies.

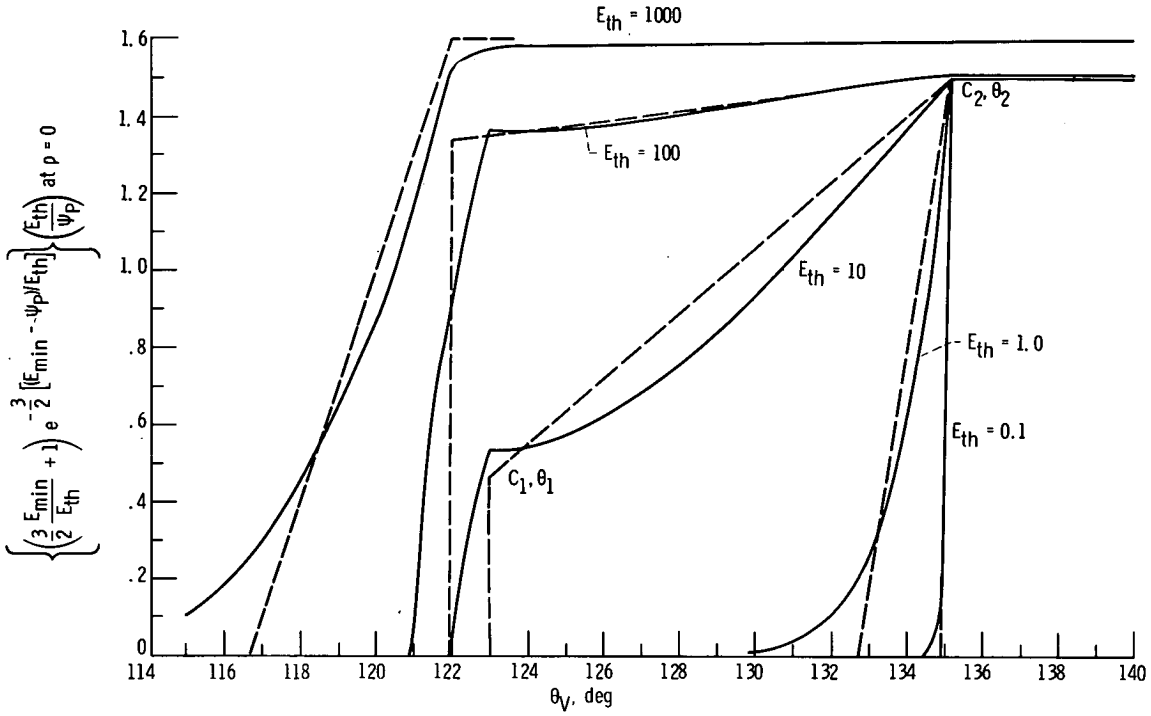

Figure 17. - Linear approximations in current collection integral.

NATIONAL AERONAUTICS AND SPACE ADMINISTRATION
WASHINGTON, D.C. 20546

OFFICIAL BUSINESS
PENALTY FOR PRIVATE USE $300

SPECIAL FOURTH-CLASS RATE
BOOK

POSTAGE AND FEES PAID
NATIONAL AERONAUTICS AND
SPACE ADMINISTRATION
451

U.S.MAIL

POSTMASTER: If Undeliverable (Section 158 Postal Manual) Do Not Return

"The aeronautical and space activities of the United States shall be conducted so as to contribute . . . to the expansion of human knowledge of phenomena in the atmosphere and space. The Administration shall provide for the widest practicable and appropriate dissemination of information concerning its activities and the results thereof."

—NATIONAL AERONAUTICS AND SPACE ACT OF 1958

NASA SCIENTIFIC AND TECHNICAL PUBLICATIONS

TECHNICAL REPORTS: Scientific and technical information considered important, complete, and a lasting contribution to existing knowledge.

TECHNICAL NOTES: Information less broad in scope but nevertheless of importance as a contribution to existing knowledge.

TECHNICAL MEMORANDUMS: Information receiving limited distribution because of preliminary data, security classification, or other reasons. Also includes conference proceedings with either limited or unlimited distribution.

CONTRACTOR REPORTS: Scientific and technical information generated under a NASA contract or grant and considered an important contribution to existing knowledge.

TECHNICAL TRANSLATIONS: Information published in a foreign language considered to merit NASA distribution in English.

SPECIAL PUBLICATIONS: Information derived from or of value to NASA activities. Publications include final reports of major projects, monographs, data compilations, handbooks, sourcebooks, and special bibliographies.

TECHNOLOGY UTILIZATION PUBLICATIONS: Information on technology used by NASA that may be of particular interest in commercial and other non-aerospace applications. Publications include Tech Briefs, Technology Utilization Reports and Technology Surveys.

Details on the availability of these publications may be obtained from:

SCIENTIFIC AND TECHNICAL INFORMATION OFFICE

NATIONAL AERONAUTICS AND SPACE ADMINISTRATION

Washington, D.C. 20546